Materials and Design 144 (2018) 310–322

Contents lists available at ScienceDirect

Materials and Design

journal homepage: www.elsevier.com/locate/matdes

Stability and elasticity of metastable solid solutions and superlattices in the MoN–TaN system: First-principles calculations

Nikola Koutná[a,b,*], David Holec[c], Martin Friák[d,e,b], Paul H. Mayrhofer[a], Mojmír Šob[e,d,f]

[a] Institute of Materials Science and Technology, TU Wien, Getreidemarkt 9, A-1060 Vienna, Austria
[b] Department of Condensed Matter Physics, Faculty of Science, Masaryk University, Kotlářská 2, Brno CZ-611 37, Czech Republic
[c] Department of Physical Metallurgy and Materials Testing, Montanuniversität Leoben, Franz-Josef-Strasse 18, Leoben A-8700, Austria
[d] Institute of Physics of Materials, Academy of Sciences of the Czech Republic, v.v.i., žižkova 22, Brno CZ-616 62, Czech Republic
[e] Central European Institute of Technology, CEITEC MU, Masaryk University, Kamenice 5, Brno CZ-625 00, Czech Republic
[f] Department of Chemistry, Faculty of Science, Masaryk University, Kotlářská 2, Brno CZ-611 37, Czech Republic

HIGHLIGHTS

- We present DFT calculations on $Mo_{1-x}Ta_xN$ solid solutions and $(MoN)_{1-x}/(TaN)_x$ superlattices.
- The most stable alloys crystallize with a hexagonal symmetry and exhibit high elastic moduli.
- The disordered fcc-based alloys are energetically and mechanically superior to their ordered counterparts.
- MoN/TaN interface leads to a stabilisation of novel tetragonal ζ-phases with an improved dynamical stability.
- The superlattices are predicted to be more ductile than the most stable hexagonal alloys.

GRAPHICAL ABSTRACT

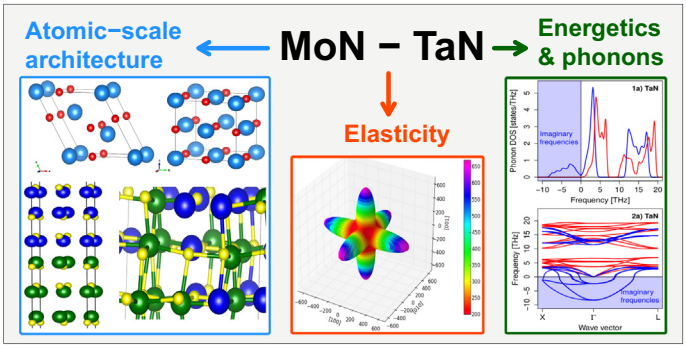

ARTICLE INFO

Article history:
Received 3 October 2017
Received in revised form 7 February 2018
Accepted 11 February 2018
Available online 14 February 2018

Keywords:
MoN-TaN
Phase stability
Symmetry
Elasticity
Electronic properties

ABSTRACT

In order to develop design rules for novel nitride-based coatings, we investigate trends in thermodynamic, structural, elastic, and electronic properties of $Mo_{1-x}Ta_xN$ single-phase alloys together with $(MoN)_{1-x}/(TaN)_x$ superlattices. Our calculations predict that hexagonal $Mo_{1-x}Ta_xN$ are the overall most stable ones, followed by the disordered cubic solid solutions and superlattices. The disordered cubic systems are energetically clearly favoured over their ordered counterparts. To explain this unexpected phenomenon, we perform an in-depth structural analysis of bond-lengths and angles, revealing that the disordered phase is structurally between the NaCl-type and the hexagonal NiAs-type modifications. Similarly, the bi-axial coherency stresses in MoN/TaN break the cubic symmetry beyond simple tetragonal distortions, leading to a new tetragonal ζ-phase (P4/nmm, #129). Both ζ-MoN and ζ-TaN have lower formation energy than their cubic counterparts. Unlike the cubic TaN, the ζ-TaN is also dynamically stable. The hexagonal alloys are predicted to be extremely hard, though, much less ductile than the cubic polymorphs and superlattices.

* Corresponding author at: Institute of Materials Science and Technology, TU Wien, Getreidemarkt 9, Vienna A-1060, Austria.
E-mail address: nikola.koutna@tuwien.ac.at (N. Koutná).

https://doi.org/10.1016/j.matdes.2018.02.033
0264-1275/

1. Introduction

Transition metal nitrides (TMNs) represent a prominent class of materials possessing numerous outstanding physical properties, such as excellent chemical and thermal stability [1, 2], incompressibility [3, 4] and strength [5, 6], high melting point, good thermal and electric conductivity or superconductivity [7–9]. In order to enhance materials performance, considerable efforts have been devoted to investigate the possibility of fine tuning the energetic, mechanical and/or electrical properties by designing ternary or multinary (T)MN systems [10–19].

The addition of nitrogen atoms into the high-density electronic gas of transition metals together with the covalent bonding leads to extraordinary hardness [20, 21]. Specifically, the hardness of MoN and TaN ranges from 28 to 34 GPa [4, 22–24]. According to Teter's empirical law [25], hardness scales with shear modulus. Later, Chen et al. [26] also correlated hardness to bulk modulus. Recent systematic DFT calculations on Ta–N [27] and Mo–N [28] system suggest that the bulk modulus can reach 338 and 347 GPa for the WC-type TaN and δ-MoN_2, respectively, which is comparable with the 370 GPa of the cubic BN [29].

TMNs often crystallize in a cubic NaCl-type structure ($Fm\bar{3}m$, #225), termed as rocksalt (rs) [30]. Despite being metastable, the cubic modifications of MoN and TaN have been synthesized using non-equilibrium growth techniques [4, 22, 31–34], e.g., reactive magnetron sputtering in high nitrogen partial pressure atmosphere, nitrogen ion implantation, or low energy ion assisted deposition. Properties of cubic MoN and TaN are comparable with, or even superior to those of the ground state phases. For example, cubic TaN prepared by shock and static compression was shown to have very good high-temperature stability, comparable to that of the hexagonal WC-type phase [33]. Moreover, experiments of Haberkorn et al. [35] suggest that the cubic MoN is very promising as a superconductor with transition temperature of 3–8 K.

Although considerable effort has been devoted to Mo–N and Ta–N, the quasi-binary MoN–TaN system has been rarely studied [36, 37]. Restricting only to cubic system, Bouamama et al. [36] performed DFT calculations on both (fully) ordered and disordered $Mo_{1-x}Ta_xN$. The virtual crystal approximation (VCA) used to model the disordered phase in their study, however, neglects any possible short range order. Therefore, it is desirable to employ more sophisticated approaches closer to reality, e.g., the special quasirandom structure (SQS) method [38].

Our work aims to reveal compositional trends in thermodynamics and elasticity of $Mo_{1-x}Ta_xN$ alloys with cubic and hexagonal symmetry. Structural models for $Mo_{1-x}Ta_xN$ are based on the NaCl-, NiAs-, WC-, and TaN-phase prototypes, representing the energetically most favourable modifications of MoN and TaN. To guide future experiments, the role of microstructure is analysed by considering (1) ordered vs. disordered alloys, and (2) different concepts of materials architecture—alloys vs. cubic-based superlattices.

2. Calculation details

The Vienna Ab-initio Simulation Package (VASP) [39, 40] was used to perform the DFT calculations, employing the projector augmented plane wave (PAW) pseudopotentials under the generalized gradient approximation (GGA) [41] with a Perdew-Burke-Ernzerhof (PBE) exchange and correlation functional [42]. The plane-wave cutoff energy was always set to 700 eV and the k-vector sampling of the Brillouin zone was checked to provide a total energy accuracy of about 10^{-3} eV/at.

The $Mo_{1-x}Ta_xN$ solid solutions were assumed to adopt the cubic structure with NaCl prototype ($Fm\bar{3}m$, #225, B1-type), often referred to as rocksalt (rs), and the hexagonal structures with NiAs ($P6_3/mmc$, #194), WC ($P\bar{6}m2$, #187), and TaN ($P\bar{6}2m$, #189) prototypes, respectively. Supercells with 64 lattice sites (32 metal and 32 nitrogen atoms) were used to model the cubic systems, while supercells consisting of total of 32, 54, and 72 lattice sites modeled the NiAs-type, WC-type, and TaN-type hexagonal systems. The Ta (Mo) atoms were distributed on the metal sublattice of bulk MoN (TaN) in a disordered manner employing the SQS method [38]. Additionally, ordered rocksalt $Mo_{1-x}Ta_xN$ structures were constructed from a conventional cubic B1 cell (8 lattice sites) containing one or two metal atoms of a different type, i.e., one or two Mo (Ta) in 8-atom TaN (MoN), and subsequently expanded to 2 × 2 × 2 supercells. Various (partially) ordered compositions were obtained from the fully ordered 2 × 2 × 2 supercells with 25% or 50% of Mo (Ta) atoms by arbitrarily replacing them by metal atoms of the other type, i.e., Ta (Mo), to obtain the desired Mo-to-Ta ratio. The 1 × 1 × 2 (bi-layer period $\lambda \approx 1$ nm), 1 × 1 × 4 ($\lambda \approx 2$ nm), 1 × 1 × 6 ($\lambda \approx 3$ nm), and 1 × 1 × 8 ($\lambda \approx 4$ nm) NaCl-type supercells consisting of an equal amount of both MoN and TaN shown in Fig. 1 served as models for MoN/TaN superlattices with (001) interfaces. These supercells were also used to model superlattices with various MoN-to-TaN ratios, i.e., $(MoN)_{1-x}/(TaN)_x$, by occupying complete atomic planes by either Mo or Ta atoms and keeping the number of interfaces per supercell. The applied periodic boundary conditions produced the superlattice geometry with a bi-layer period in the range of about 0.9–3.8 nm.

Lattice parameters of the binary bulk MoN and TaN in the NaCl-, NiAs-, WC-, and TaN-type modifications were optimized by fitting the energy versus volume data with the Birch-Murnaghan equation

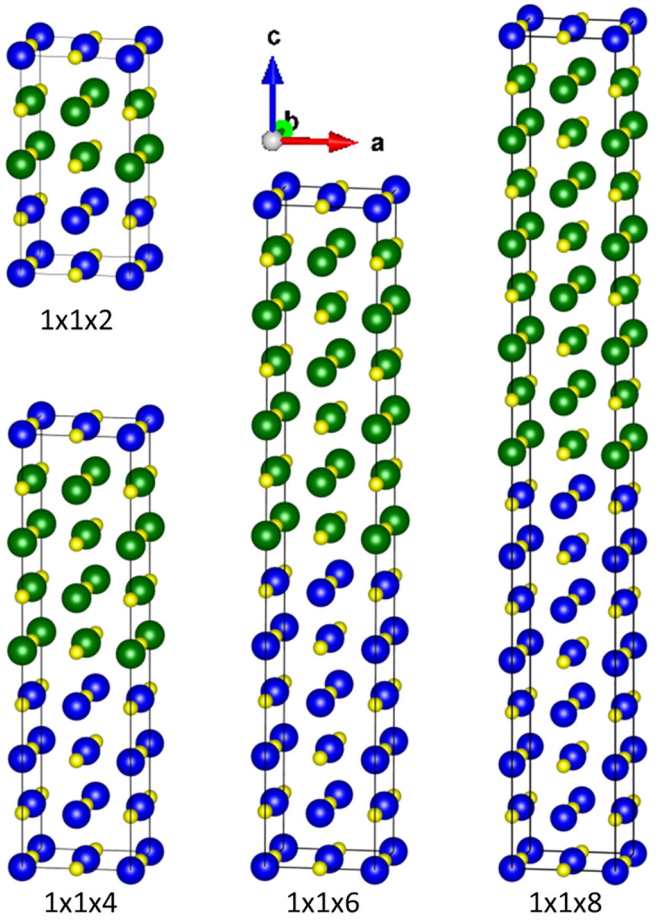

Fig. 1. Computational models for 1 × 1 × 2, 1 × 1 × 4, 1 × 1 × 6, and 1 × 1 × 8 NaCl-type MoN/TaN superlattices. The yellow, green, and blue spheres correspond to N, Ta, and Mo atoms, respectively. Visualized using the VESTA package [43–45]. (For interpretation of the references to color in this figure legend, the reader is referred to the web version of this article.)

of state [46], while all structure optimizations in the $Mo_{1-x}Ta_xN$ and $(MoN)_{1-x}/(TaN)_x$ systems were carried out by relaxing supercell volumes, shapes, and atomic positions.

To compare various systems in terms of their thermodynamic stability, energy of formation, E_f, was calculated as

$$E_f = \frac{1}{\sum_s n_s}\left(E_{\text{tot}} - \sum_s n_s \mu_s\right) \tag{1}$$

where E_{tot} is the total energy of the supercell, n_s and μ_s are the number of atoms and the chemical potential, respectively, of a species s. The reference chemical potentials for Mo, Ta, and N are conventionally set to the total energy per atom of bcc-Mo, μ_{Mo}, bcc-Ta, μ_{Ta}, and N_2 molecule, μ_{N}, respectively. The mixing enthalpy, H_{mix}, was evaluated according to

$$H_{\text{mix}} = E_f - (1-x)E_f^{\text{MoN}} - xE_f^{\text{TaN}} \tag{2}$$

where E_f^{MoN} and E_f^{TaN} are the formation energies corresponding to reference boundary states. To find out the thermodynamics of the $(MoN)_{1-x}/(TaN)_x$ superlattices, the interface energy, E_{int}, was calculated as

$$E_{\text{int}} = \frac{1}{2A}\left(E_{\text{tot}} - E_{\text{tot}}^{\text{MoN}} - E_{\text{tot}}^{\text{TaN}}\right), \tag{3}$$

where A is the area of the MoN/TaN interface and $E_{\text{tot}}^{\text{MoN}}$ ($E_{\text{tot}}^{\text{TaN}}$) is the total energy of MoN (TaN) equivalent to that used as a building block in MoN/TaN superlattice.

Furthermore, we investigated elasticity of selected $Mo_{1-x}Ta_xN$ and $(MoN)_{1-x}/(TaN)_x$ systems employing the stress-strain method [47, 48]. Fourth-order elasticity tensor $\mathbb{C}$ relates stress, σ, linearly to strain, ε, according to the Hooke's law

$$\sigma = \mathbb{C}\varepsilon. \tag{4}$$

We note that instead of using fourth-order tensor $\mathbb{C}$ in a three-dimensional space, it is often convenient to replace it with a 6×6 matrix. In the following, $\mathbb{C}$ will represent this matrix of elastic constants in the so-called Voigt's notation. To evaluate elastic constants corresponding to structures with arbitrary symmetry, we adopt the methodology proposed by Moakher and Norris [49]. First, the squared norm of the elasticity matrix $\mathbb{C}$ is defined as

$$\|\mathbb{C}\|^2 := \langle \mathbb{C}, \mathbb{C} \rangle. \tag{5}$$

The scalar product $\langle \mathbb{C}, \mathbb{C} \rangle$ can be calculated in various ways depending on how $\mathbb{C}$ is represented. Assuming the Euclidean metrics and the case of 2D representation, Eq. (5) takes form

$$\|\mathbb{C}\|^2 = \sum_{i,j=1}^{6} C_{ij}^2 \quad . \tag{6}$$

Aiming to simplify the general 6×6 matrix $\mathbb{C} = (C_{ij})$ with 21 independent elements, we wish to project it onto a convenient symmetry class and hence, decrease the number of independent elastic constants. Thus we search for a matrix $\mathbb{C}_{\text{sym}}$ of a specific symmetry class such that the norm

$$\|\mathbb{C} - \mathbb{C}_{\text{sym}}\| \tag{7}$$

is minimal. In other words, we minimize the Euclidean distance between the matrix of elastic constants, $\mathbb{C}$, with an arbitrary symmetry and the elasticity matrix $\mathbb{C}_{\text{sym}}$ of some particular symmetry. Rigorous derivation of the projectors for all crystal symmetry classes can be found in Refs. [49] and [50]. Furthermore, according to Mouhat and Coudert [51], mechanical stability of a system with an arbitrary symmetry is mathematically equivalent with any of the following necessary and sufficient conditions:

(i) the matrix $\mathbb{C}$ is positive definite,
(ii) all eigenvalues of $\mathbb{C}$ are positive,
(iii) all the leading principal minors of $\mathbb{C}$ are positive,
(iv) any minor of $\mathbb{C}$ is positive.

Finally, we calculate phonon spectra of selected systems using the Phonopy package [52].

3. Results and discussion

3.1. Thermodynamic stability

Fig. 2 depicts the energy of formation, E_f, as a function of Ta content in MoN/TaN superlattices and MoTaN alloys adopting cubic (ordered/disordered) or hexagonal (NiAs-, TaN-, or WC-type) structure. The hexagonal polymorphs are clearly preferred along the MoN–TaN quasi-binary tie-line, i.e., with fully occupied metal and nitrogen sublattices. In particular, $Mo_{1-x}Ta_xN$ is predicted to adopt the NiAs-, WC-, and TaN-type structure for x in intervals of ~(0,0.3), ~(0.3,0.9), and ~(0.9,1), respectively. Very close E_f values corresponding to the TaN- and WC-type phase for x in the interval of ~(0.9,1) suggest their possible coexistence for high Ta contents. When restricting to the cubic-like systems, fully disordered alloys (constructed according to the SQS method) exhibit the lowest E_f, closely followed by the superlattices, especially for the Ta-rich compositions. The partially ordered cubic $Mo_{1-x}Ta_xN$ is predicted to be the least stable out of the here considered structures.

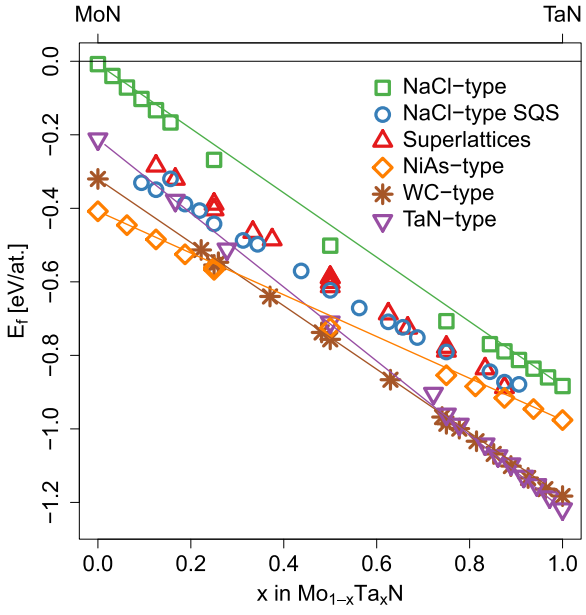

Fig. 2. Energy of formation, E_f, as a function of x in $Mo_{1-x}Ta_xN$. Solid solutions adopt the cubic NaCl-type, and the hexagonal NiAs-, WC-, and TaN-type phases, while the superlattices are based on the NaCl structure. The straight lines connect E_f of the bulk MoN and TaN with the same prototype.

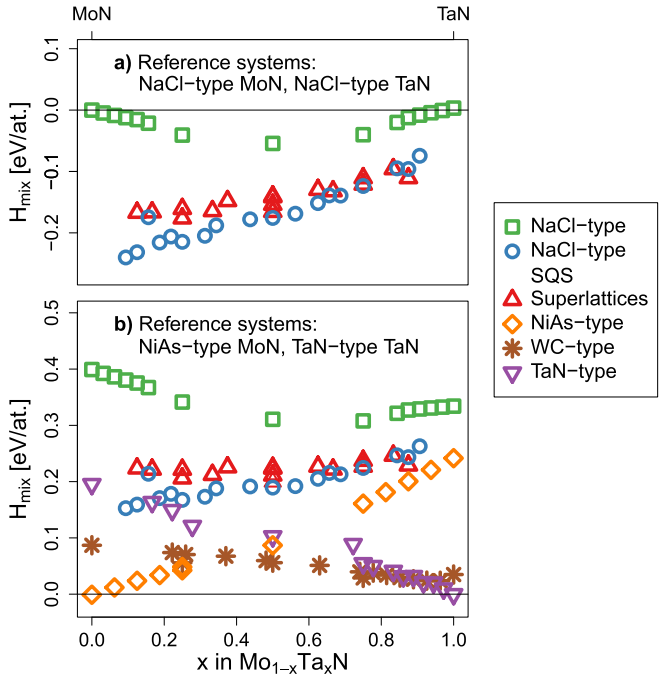

Fig. 3. Mixing enthalpy, H_{mix}, as a function of x in $Mo_{1-x}Ta_xN$. In panel a), the data points are evaluated with respect to the NaCl-type structures, while in panel b) the zero mixing enthalpy corresponds to ground states of MoN and TaN, i.e., the NiAs-type MoN and the TaN-type TaN.

The parent lattice used to construct disordered and ordered solid solutions as well as the superlattices, was the cubic rocksalt structure. Consequently, evaluating mixing enthalpy, H_{mix}, according to Eq. (2) with respect to the NaCl-type MoN and TaN quantifies the thermodynamic driving force for isostructural (spinodal) decomposition (Fig. 3a). It follows that all these systems exhibit negative mixing enthalpy and hence are stable against isostructural decomposition. However, since the cubic binary polymorphs are not the respective ground states of MoN and TaN (cf. Fig. 2), in Fig. 3b we plot H_{mix} evaluated with respect to the hexagonal NiAs-type MoN and the TaN-type TaN, the most stable polymorphs of the binary boundary systems. Here, H_{mix} does no longer quantify driving for isostructural decomposition, but simply a stability of the quasi-binary system with respect to the most stable reference systems. Therefore, also the hexagonal solid solutions were considered. Our results indicate that all $Mo_{1-x}Ta_xN$ solid solutions together with $(MoN)_{1-x}/(TaN)_x$ superlattices are unstable with respect to the respective ground state hexagonal phases. The calculated H_{mix} values are in a similar range as for other nitride systems (e.g., $Ti_{1-x}Al_xN$ or $Zr_{1-x}Al_xN$) known to decompose upon thermal loading [1].

3.2. Structural analysis of ordered and disordered solid solutions

The shape of the H_{mix} curve for the disordered cubic solid solution is somehow surprising, because it shows an almost linear compositional dependence, which suggests a significant deviation from $H_{\mathrm{mix}} = 0$ when extrapolated to $x = 0$ (cf. Fig. 3a). In isostructural case, however, H_{mix} should be 0 for $x = 0$ and $x = 1$ according to Eq. (2). A possible origin of such deviation might be that due to atomic relaxations in the solid solution, the structure is significantly modified. Hence, H_{mix} evaluated with respect to the NaCl-type boundary binaries does not represent an isostructural case. Analysis of fully relaxed NaCl-type alloys reveals that their specific volumes, V(NaCl-type $Mo_{1-x}Ta_xN$), follow the Vegard's-like linear relationship [53, 54], i.e.,

$$V(\text{NaCl-type } Mo_{1-x}Ta_xN) \approx (1-x)V(\text{NaCl-type MoN}) + xV(\text{NaCl-type TaN}), \tag{8}$$

where V(NaCl-type MoN) and V(NaCl-type TaN) are specific volumes of the NaCl-type MoN and TaN, respectively. Analogically, volumes of the hexagonal systems lie very close to the line connecting the respective hexagonal binary boundaries. This result suggests that if the disordered NaCl-type systems significantly deviate from the perfect cubic structure, such deviation has to be local. Consequently, we analyse local environments of the ordered and disordered solid solutions and compare them with the cubic NaCl-type and the hexagonal NiAs-, WC-, and TaN-type phases of MoN and TaN. A common attribute of all these polymorphs is that every metal atom has 6 nearest N neighbours. Hence, 6 distances, $d_1, d_2 \ldots, d_6$, and 15 angles, $\varphi_1, \varphi_2, \ldots, \varphi_{15}$ between every (central) metal atom and its nearest N neighbours can be determined, and ordered ascendingly, i.e., in such way that $d_1 \le d_2 \le \ldots \le d_6$ and $\varphi_1 \le \varphi_2 \le \ldots \le \varphi_{15}$.

Let us introduce the ith lowest averaged distance, D_i,

$$D_i := \frac{1}{M}\sum_{j=1}^{M} d_i^{\mathrm{at}j} = \mathrm{mean}\left(d_i^{\mathrm{at}1}, d_i^{\mathrm{at}2}, \ldots, d_i^{\mathrm{at}M}\right), \tag{9}$$

where $d_i^{\mathrm{at}j}$ denotes the ith lowest distance corresponding to the jth metal atom in the supercell, i.e., the distance between the jth metal atom and its ith nearest nitrogen neighbour. M is the number of metal atoms included in the analysis. Similarly, the kth lowest averaged angle, ϕ_k, takes form

$$\phi_k := \frac{1}{M}\sum_{j=1}^{M} \varphi_k^{\mathrm{at}j} = \mathrm{mean}\left(\varphi_k^{\mathrm{at}1}, \varphi_k^{\mathrm{at}2}, \ldots, \varphi_k^{\mathrm{at}M}\right), \tag{10}$$

where $\phi_k^{\mathrm{at}j}$ denotes the kth lowest angle corresponding to the jth metal atom in the supercell. To quantify the structural (dis)similarity of the disordered cubic $Mo_{1-x}Ta_xN$ solid solutions with binary prototypes, we further define

$$\Delta\mathrm{Dist} := \frac{1}{6}\sum_{i=1}^{6}\frac{\left|D_i - D_i^{\mathrm{Ref}}\right|}{D_i^{\mathrm{Ref}}} = \mathrm{mean}\left(\frac{\left|D_1 - D_1^{\mathrm{Ref}}\right|}{D_1^{\mathrm{Ref}}}, \ldots, \frac{\left|D_6 - D_6^{\mathrm{Ref}}\right|}{D_6^{\mathrm{Ref}}}\right), \tag{11}$$

where D_i and D_i^{Ref} correspond to the ith lowest averaged distance in the cubic solid solution and in a reference structure, respectively, while the summation runs over all 6 averaged distances. Analogically, we introduce

$$\Delta\mathrm{Angles} := \frac{1}{15}\sum_{k=1}^{15}\frac{\left|\phi_k - \phi_k^{\mathrm{Ref}}\right|}{\phi_k^{\mathrm{Ref}}} = \mathrm{mean}\left(\frac{\left|\phi_1 - \phi_1^{\mathrm{Ref}}\right|}{\phi_1^{\mathrm{Ref}}}, \ldots, \frac{\left|\phi_{15} - \phi_{15}^{\mathrm{Ref}}\right|}{\phi_{15}^{\mathrm{Ref}}}\right), \tag{12}$$

where ϕ_k and ϕ_k^{Ref} denote the kth lowest averaged angle in the cubic solid solution and in a reference system, respectively, and the summation runs over all 15 averaged angles. It is important to mention that the local environments of Mo and Ta atoms in $Mo_{1-x}Ta_xN$ were

analysed separately, i.e., M in Eqs. (9) and (10), was either the number of Mo or Ta atoms; the later (former) case was compared with local environments in binary MoN (TaN) in a corresponding reference structure.

Results of the analysis according to Eqs. (11) and (12) are plotted in Fig. 4. The first interesting observation is that the angles in disordered $Mo_{1-x}Ta_xN$ differ from all binary systems by about 4–15%, thus much more significantly than the distances, which differ by 1–5%. Regarding ΔAngles, the lowest values ~5% are obtained when evaluated with respect to NiAs-type structure, the ground state of MoN. Nevertheless, evaluation with respect to cubic NaCl-type polymorph yields very close values as well, with ΔAngles between 6 to 7%. On the contrary, evaluation with respect to WC-type and TaN-type phases results in significantly higher ΔAngles of ~15%, and hence, we conclude that the angles in disordered $Mo_{1-x}Ta_xN$ are rather dissimilar to these two hexagonal modifications. Moreover, the trends are supported also by error bars, which are relatively small for the NiAs- and NaCl-type reference systems, but are almost doubled when referring to the WC- and TaN-type polymorphs. We note that the φ_k angles are 90° or 180° in the cubic rocksalt structure, while they take values of ~82°, 98°, and 180° in the NiAs-type structure, ~80°, 84°, and 136° in the TaN-type structure, and ~82°, and 136° in the WC-type structure. Unlike that, φ_ks in the disordered $Mo_{1-x}Ta_xN$ are changing gradually from ~77° to ~105°, independent of the composition x. Unfortunately, ΔDist cannot be interpreted that easily, since all the values are rather small and comparable, regardless of the reference structure. While D_is evaluated in any of the binary reference structures yield the same value for each system due to the symmetries, the disordered $Mo_{1-x}Ta_xN$ is characterized by six distinct D_is stemming from the local structural relaxations. Nevertheless, the best agreement (by a small margin regarding both the ΔDist values as well as the error-bars) is obtained again for the cubic NaCl-type and the hexagonal NiAs-type phase, especially for the Ta atoms.

Therefore, our structural analysis of the disordered cubic $Mo_{1-x}Ta_xN$ solid solution shows that the symmetries of a rocksalt lattice are broken due to the chemical disorder. Consequently, the

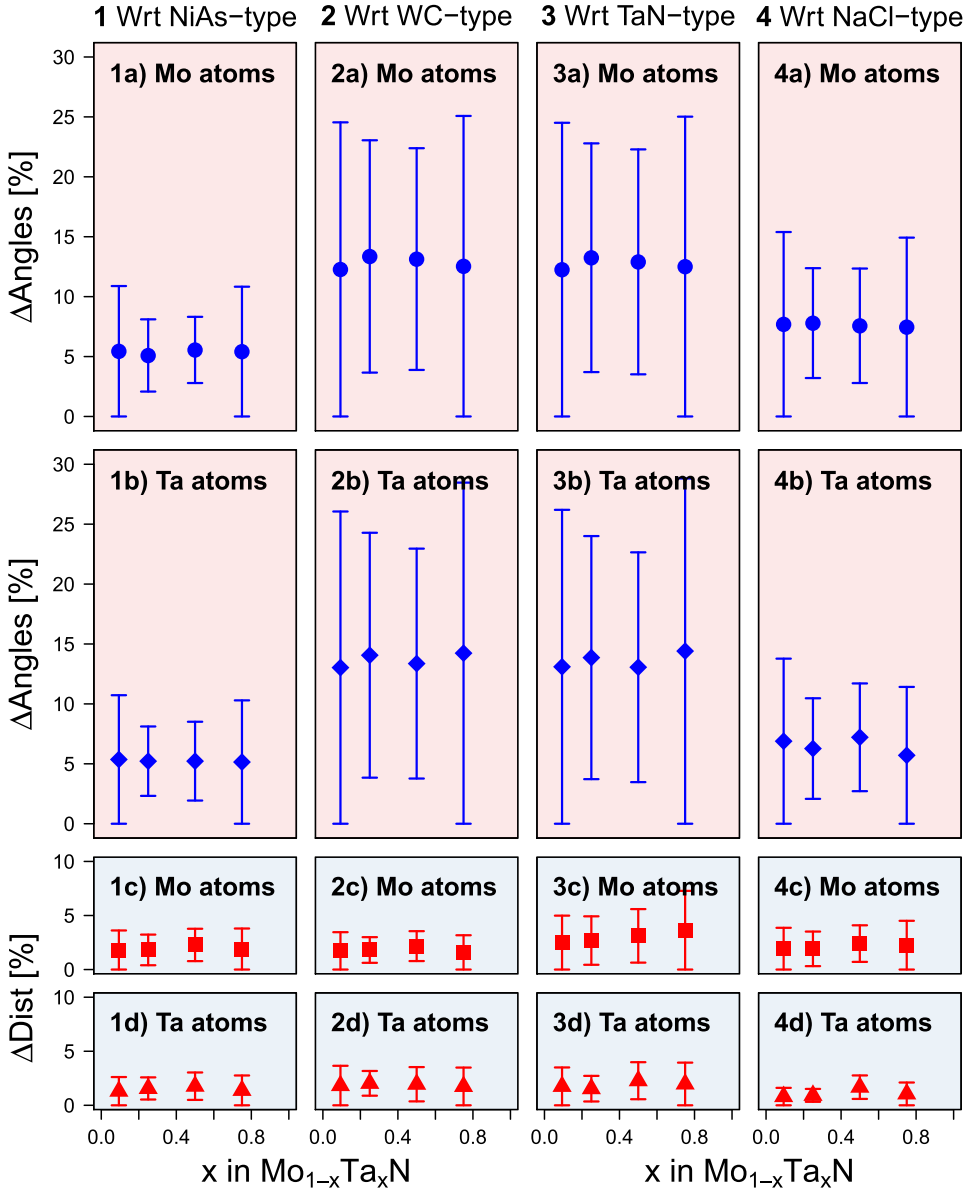

Fig. 4. The averaged differences of angles (8 upper panels) and distances (8 lower panels) as a function of x in $Mo_{1-x}Ta_xN$. The data evaluated with respect to the hexagonal NiAs-, WC-, TaN-type and the cubic NaCl-type structure are depicted in panels 1a)–1d), 2a)–2d), 3a)–3d), and 4a)–4d), respectively. The error bars are calculated as standard deviations.

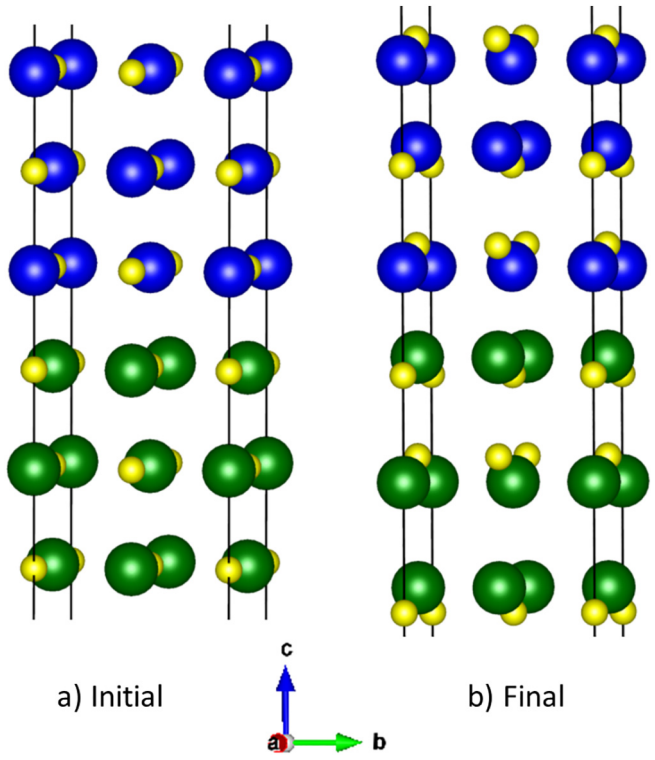

Fig. 5. Snapshot of (a) the initial and (b) corresponding fully relaxed structure of a MoN/TaN superlattice. The yellow, green, and blue spheres correspond to N, Ta, and Mo atoms, respectively. Visualized using the VESTA package [43–45].

disordered phase is structurally between the cubic NaCl-type and the hexagonal NiAs-type modifications. This rationalizes the peculiar compositional dependence of E_f corresponding to the disordered cubic $Mo_{1-x}Ta_xN$ (Fig. 2), which is almost perfectly between the E_f values of the (partially) ordered cubic and the NiAs-type hexagonal systems.

3.3. Superlattice architecture

The energy of formation of the $(MoN)_{1-x}/(TaN)_x$ superlattices was predicted to lie close to E_f of the disordered $Mo_{1-x}Ta_xN$ solid solutions (Fig. 2). Furthermore, the corresponding interface energies, E_{int}, are negative with respect to the cubic phases. These hints indicate that again the symmetries are (partially) broken, i.e., the superlattices are not composed of simply tetragonally-deformed cubic cells. Indeed, a further analysis of fully relaxed $(MoN)_{1-x}/(TaN)_x$ reveals not only a tetragonal deformation (Fig. 5), but also additional atomic displacements, which further break the tetragonal symmetry.

The tetragonal-like structures of the two binaries, MoN and TaN, were constructed out of $1 \times 1 \times 2$ MoN/TaN superlattice, and were fully relaxed until the forces on individual atoms were less than 0.01 eV/Å. A subsequent structural analysis showed that both these newly proposed phases of MoN and TaN, which will be hereafter referred to as ζ-MoN and ζ-TaN, possess the space group P4/nmm (#129). The corresponding lattice parameters together with the atomic positions are summarized in Table I. The calculated formation energies of ζ-MoN and ζ-TaN are −0.178 eV/at. and −0.982 eV/at., respectively. Therefore, the ζ-phase is predicted to be thermodynamically more stable than the rocksalt structure for both MoN and TaN, exhibiting E_f of −0.008 eV/at. and −0.887 eV/at., respectively.

In order to reveal the driving force for the tetragonal distortion leading to the cubic-to-ζ transition in MoN and TaN, we calculated their phonon spectra (Fig. 6). The phonon density of states and phonon dispersion relation of ζ-TaN do not show any imaginary phonon frequencies (unlike in the case of rs-TaN), hence imply also its mechanical stability (which was further confirmed by testing that the corresponding matrix of elastic constants is positive definite, see Section 3.4). Further relaxation following the soft phonon modes in ζ-MoN leads to another low-symmetry structure, a monoclinic ω-MoN ($P2_1/m$, #11) with E_f of about −0.2454 eV/at, therefore, comparable to that of rs-$Mo_{0.91}N$ [55]. However, this phase is not relevant for the superlattices as it is forbidden by the superlattice tetragonal symmetry.

The interface energy, E_{int} of the $(MoN)_{1-x}/(TaN)_x$ superlattices, evaluated with respect to our newly proposed ζ-TaN and ζ-MoN is close to 0 eV/Å^2. Moreover, E_{int} becomes positive, when evaluated with respect to ζ-TaN and ω-MoN. Such values of E_{int} can be better physically interpreted and agree well with the previously discussed thermodynamic stability (cf. Fig. 2).

3.4. Elastic properties

Tensors of elastic properties represented using symmetrical 6×6 matrices $\mathbb{C}$ were calculated for selected $Mo_{1-x}Ta_xN$ systems at 5 different compositions, namely, for $x \in \{0, 0.25, 0.5, 0.75, 1\}$. As these systems belong to different crystal symmetry classes, and moreover, their symmetries are often broken due to the chemical disorder and/or architecture, it is desirable to pay special attention to unifying the method for analysing their elastic response. Therefore, the mechanical stability was tested employing the condition (iii) in Section 2, i.e., that the lowest eigenvalue, λ_{min}, corresponding to the (unprojected) matrix $\mathbb{C}$, must be positive.

The results presented in Fig. 7a reveal that all hexagonal $Mo_{1-x}Ta_xN$ phases are mechanically stable in the whole compositional range, i.e., the corresponding λ_{min} is always positive. Mechanical stability of the ordered cubic variant depends strongly on the Ta content. This finding is consistent with the previous ab initio study by Bouamama et al. [36] showing that ordered cubic $Mo_{1-x}Ta_xN$ becomes stable for $x > 0.27$. On the contrary, the disordered $Mo_{1-x}Ta_xN$ is predicted to be stabilized by introducing

Table I
Overview of lattice parameters, a and c, and atomic coordinates (x, y, z) of the newly identified ζ-MoN and ζ-TaN phases.

ζ-MoN			ζ-TaN		
a, c [Å]	Atom	(x, y, z)	a, c [Å]	Atom	(x, y, z)
$a = 4.2480$	Mo1	(0.0000, 0.0000, 0.0150)	$a = 4.2017$	Ta1	(0.0000, 0.0000, 0.9975)
$c = 4.5435$	Mo2	(0.0000, 0.0000, 0.4353)	$c = 5.1188$	Ta2	(0.0000, 0.5000, 0.4525)
	Mo3	(0.5000, 0.0000, 0.4353)		Ta3	(0.5000, 0.0000, 0.4525)
	Mo4	(0.5000, 0.5000, 0.0150)		Ta4	(0.5000, 0.5000, 0.9975)
	N1	(0.5000, 0.5000, 0.5311)		N1	(0.5000, 0.5000, 0.5592)
	N2	(0.5000, 0.0000, 0.9186)		N2	(0.5000, 0.0000, 0.8907)
	N3	(0.0000, 0.5000, 0.9186)		N3	(0.0000, 0.5000, 0.8907)
	N4	(0.0000, 0.0000, 0.5311)		N4	(0.0000, 0.0000, 0.5592)

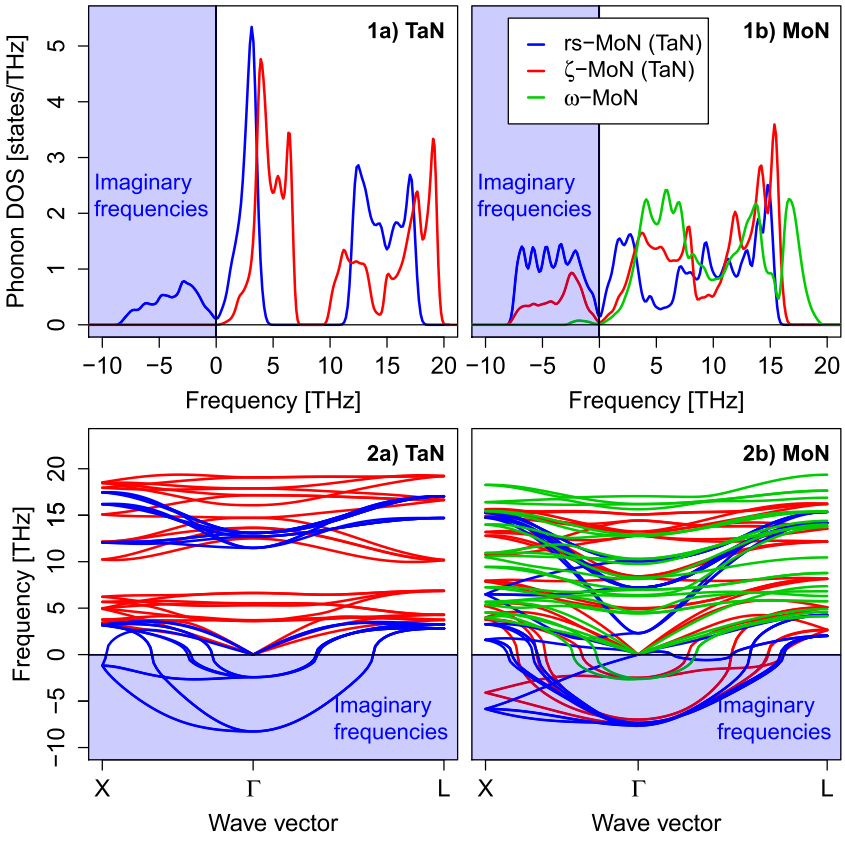

Fig. 6. Phonon density of states, panels 1a)–b), and phonon dispersions, panels 2a)–2b), for MoN and TaN adopting the rocksalt (blue lines), tetragonal ζ-type (red lines), and monoclinic ω-type (green lines) structures. (For interpretation of the references to color in this figure legend, the reader is referred to the web version of this article.)

already ~10% of Ta, i.e., for $x \geq 0.1$, which again highlights a strong stabilizing role of the chemical disorder in rocksalt structure. Comparable phenomena of stabilizing effects of chemical disorder have been recently shown also for TiAl intermetallic alloys [56]. Besides, trends similar to the ordered cubic $Mo_{1-x}Ta_xN$ were predicted in the case of $(MoN)_{1-x}/(TaN)_x$ superlattices, which yield $\lambda_{min} > 0$ for TaN fractions ≥50%. Nevertheless, their mechanical stability strongly depends on the actual bi-layer period: considering a TaN-to-MoN ratio of 1:1, the 1 × 1 × 2 superlattice is unstable, the 1 × 1 × 4 superlattice is stable, while the 1 × 1 × 6 superlattice is again close to instability. It should be pointed out that all the here-considered modifications of TaN, including the newly proposed tetragonal ζ-TaN, are mechanically stable. Unlike that, MoN is predicted to be stable in the hexagonal NiAs-type and WC-type structures, but unstable in the rocksalt and the tetragonal ζ-type modifications, and nearly unstable ($\lambda_{min} \sim 0$) in the hexagonal TaN-type structure (the ground state of TaN).

In order to decrease the number of generally 21 independent elastic constants (being a consequence of the low symmetry originating from the local chemical disorder), we search for the closest tensor $\mathbb{C}_{sym}$ with a higher symmetry. This is done by minimizing the Euclidean distance $\|\mathbb{C}-\mathbb{C}_{sym}\|$ (cf. Eq. (7)), thereby representing the best projection of $\mathbb{C}$. In total we considered three symmetries: cubic, tetragonal, and hexagonal, while the corresponding projections were denoted by $\mathbb{C}_{cub}$, $\mathbb{C}_{tetr}$, and $\mathbb{C}_{hex}$, respectively (Fig. 7b–d). It follows that the ordered $Mo_{1-x}Ta_xN$ is either cubic, or tetragonal. The similarity to tetragonal structure may appear surprising at the first sight, but can be easily related to the structural order. Moreover, $\mathbb{C}_{tetr}$ has 3 additional degrees of freedom in comparison with $\mathbb{C}_{cub}$, i.e., $C_{23} \neq C_{12}$, $C_{33} \neq C_{11}$, and $C_{66} \neq C_{44}$, hence, tetragonal projection can minimize distance from $\mathbb{C}$ of cubic system, but the cubic projection will never minimize the distance from $\mathbb{C}$ of tetragonal system. As a consequence of further reducing the crystal symmetry, e.g., to orthorhombic ($\mathbb{C}_{orth}$), monoclinic ($\mathbb{C}_{mon}$) or triclinic ($\mathbb{C}_{tri}$), the corresponding Euclidean distance can get even smaller. Regarding the disordered $Mo_{1-x}Ta_xN$, the norm $\|\mathbb{C}-\mathbb{C}_{sym}\|$ does not exhibit any pronounced minimum for either of the high symmetry classes, i.e., $\mathbb{C}_{cub}$, $\mathbb{C}_{hex}$, and $\mathbb{C}_{tetr}$, as it generally yields "distance" 50–150 GPa regardless of the Ta concentration. Interestingly, the distances from $\mathbb{C}_{orth}$, $\mathbb{C}_{mon}$, and $\mathbb{C}_{tri}$ of about 40–100 GPa are also non-negligible. This can be interpreted as a sign of broken symmetry, thus supporting our previous conclusions. In the case of hexagonal systems, the calculated elastic tensors exhibit large deviations from a strict cubic symmetry, but are very close to hexagonal and tetragonal symmetry. The latter is a consequence of the fact that an elastic tensor with the hexagonal symmetry may be viewed as a special case of the tetragonal symmetry [57]. Regarding $(MoN)_{1-x}/(TaN)_x$ superlattices, projection onto tetragonal symmetry class is clearly favoured over the cubic and hexagonal ones, and this trend becomes more pronounced with increasing Ta concentration, i.e., $\|\mathbb{C}-\mathbb{C}_{tetr}\|$ decreases from 135 GPa (ζ-MoN) to 12 GPa (ζ-TaN).

Based on this analysis, the calculated elastic tensors were projected onto the closest tensor of higher symmetry class, excluding trigonal, orthorhombic, monoclinic and triclinic symmetry, and the results are listed in Table II. Elastic constants corresponding to the binary MoN and TaN systems are in agreement with the previously published values.

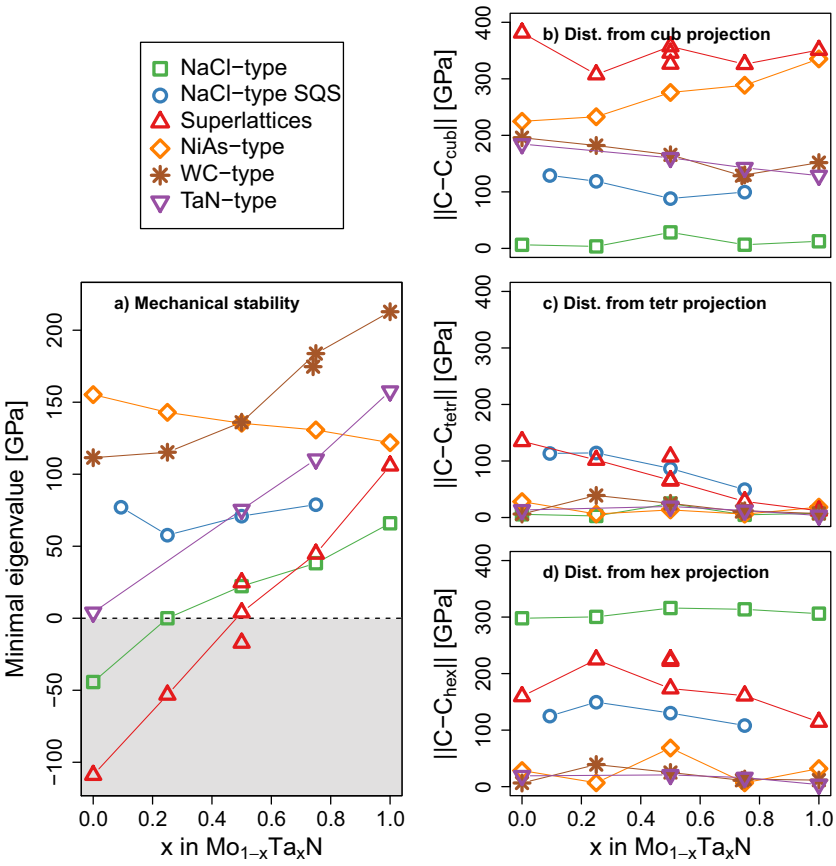

Fig. 7. Properties of the elastic tensor corresponding to the $Mo_{1-x}Ta_xN$ solid solutions and $(MoN)_{1-x}/(TaN)_x$ superlattices: minimal eigenvalue (a) together with the distance from cubic (b), tetragonal (c), and hexagonal projection (d).

Finally, we calculated the polycrystalline bulk (B), shear (G), and Young's moduli (E) using the projected elastic tensors. We represent them with the Hill's average [65] of the upper bounds according to the Reuss's approach (subscript "R") [66] and the lower Voigt's bounds (subscript "V") [67]. General formulae for R and V estimates of B and G can be found in Ref. [68]. Young's modulus was evaluated as

$$E = \frac{9BG}{3B + G}. \tag{13}$$

The compositional dependence of B, G, and E (Fig. 8) for the ordered cubic $Mo_{1-x}Ta_xN$ are in good agreement with previous ab initio study by Bouamama et al. [36] reporting that their bulk modulus slightly increases from 306 GPa (MoN) to 373 GPa (TaN). Our calculations yield an increase in B from 325 GPa (MoN) to 340 GPa (TaN), which agrees better with the 347 GPa obtained for NaCl-type TaN by Zhao et al. [63]. The hexagonal NiAs-type and WC-type structures show slightly higher B values. Specifically, B of the NiAs-structured MoN is approximately 350 GPa, which is comparable with 370 GPa reported for the cubic boron nitride (c-BN) [29], the second hardest material to date. The bulk moduli of the disordered cubic-like solid solutions are about 30 GPa below those of the ordered modifications, but comparable to the hexagonal TaN-type system. The disordered cubic-like alloys exhibit almost the same shear moduli, G, of ~110 GPa, regardless of their Ta content; all other systems show an increase of G with increasing Ta content. The shear moduli increase from 188, 165 and 34 GPa to 204, 239 and 182 GPa in the case of NiAs-, WC- and TaN-type phases, respectively. Here, especially the ordered cubic phase shows a steep increase in G from 44 to 126 GPa when increasing the metal-fraction of Ta from 25 at.% (i.e., $Mo_{0.75}Ta_{0.25}N$) to 100 at.% (i.e., TaN), which is in good agreement with Bouamama et al. [36].

The Young's moduli, E, show comparable changes with the composition as the shear moduli, and increase for the hexagonal NiAs-, WC-, and TaN-type systems from 474, 428 and 98 GPa to 507, 580 and 456 GPa in the case of NiAs-, WC-, and TaN-type system, respectively. The disordered solid solutions exhibit nearly the same E moduli with ~294 GPa for all compositions. Contrary, the ordered cubic phases show a significant increase in E from 125 to 338 GPa, when increasing the metal-fraction of Ta from 25 at.% (i.e.,$Mo_{0.75}Ta_{0.25}N$) to 100 at.% (TaN). Although E_f of the hexagonal NiAs-, WC- and TaN structured $Mo_{1-x}Ta_xN$ polymorphs are similar for $x = 0.5$ (cf. Fig. 2), only the latter two exhibit the highest (and comparable) B, G, and E moduli. Unlike that, elastic moduli of the TaN-type can be rather compared to the ordered cubic systems and superlattices, which can be rationalized by the fact that MoN in the TaN-type structure is almost mechanically unstable.

To rate the ductile/brittle behavior of our MoN–TaN systems, we used the B/G ratio proposed by Pugh [69] (also termed as Pugh's ratio). The higher the B/G ratio is, the more ductile the material behaves; the critical value separating ductile and brittle materials is ~1.75 [69]. Here, especially the $(MoN)_{1-x}/(TaN)_x$ superlattices are highly interesting: although they exhibit the lowest B, G, and E moduli, they are relatively ductile with B/G of 4.70 (1 × 1 × 6 superlattice) and 3.35 (1 × 1 × 4 superlattice) for $x = 0.5$, i.e., for equally thick TaN and MoN layers. Their ductility in terms of B/G is comparable to that of the ordered rocksalt solid solutions. The disordered cubic alloys exhibit lower B/G ratios for Ta contents above 0.5, but especially at the Mo-rich side (where the ordered alloys and superlattices

Table II
The projected elastic tensors (in GPa) of the $Mo_{1-x}Ta_xN$ systems and $(MoN)_{1-x}/(TaN)_x$ superlattices together with B, G, E moduli (in GPa), Pugh's ratio, B/G, and Poisson's ratio, ν. The upper indices "ref, th" ("ref, exp") denote theoretical (experimental) references.

Phase	x	c_{11}	$c_{11}^{\text{ref, th}}$	c_{12}	$c_{12}^{\text{ref, th}}$	c_{13}	$c_{13}^{\text{ref, th}}$	c_{33}	$c_{33}^{\text{ref, th}}$	c_{44}	$c_{44}^{\text{ref, th}}$	B	$B^{\text{ref, th}}$	$B^{\text{ref, exp}}$	G	$G^{\text{ref, th}}$	E	$E^{\text{ref, th}}$	B/G	$B/G^{\text{ref, th}}$	ν	$\nu^{\text{ref, th}}$
NaCl-type	0	549	551 [58] 543 [59]	212	255 [58] 171 [59]					−43	−49 [58] −73 [59]	–			–		–		–		–	
	0.25	612		186						1		328			44		125		7.52		0.44	
	0.5	651		169						24		329			74		205		4.48		0.40	
	0.75	687		158						39		331			93		256		3.55		0.37	
	1	724	898 [60] 678 [61]	147	131 [60] 119 [61]					67	64 [60] 46 [61]	340	389 [60] 306 [61]		127	144 [60] 139 [61]	338	384 [60] 642 [61]	2.69	2.69 [60] 2.20 [61]	0.33	0.34 [60] 0.15 [61]
NaCl-type SQS	0.09	469		219						99		302			109		291		2.78		0.34	
	0.25	513		192						94		299			116		209		2.57		0.33	
	0.5	519		205						87		309			110		296		2.81		0.34	
	0.75	494		227						87		316			103		279		3.06		0.35	
ζ-type	0	465		144		250		454		−99		–			–		–		–		–	
	1	727		160		154		343		108		286			159		403		1.79		0.26	
1 × 1 × 2 superlattice	0.5	689		114		232		440		−9		–			–		–		–		–	
1 × 1 × 4 superlattice	0.5	696		170		173		407		27		305			91		248		3.35		0.36	
1 × 1 × 6 superlattice	0.25	655		198		172		421		−45		–			–		–		–		–	
	0.5	651		156		191		306		8		282			60		168		4.70		0.40	
	0.75	698		163		173		364		147		296			108		289		2.74		0.34	
NiAs-type	0	491	603 [58]	180	200 [58]	250	205 [58]	681	810 [58]	241	289 [58]	329	356 [58]	345 [62]	188	246 [58]	474	600 [58]	1.74	1.45 [58]	0.26	0.22 [58]
	0.25	505		226		220		746		240		332			173		442		1.91		0.28	
	0.5	519		254		193		764		234		340			189		479		1.80		0.27	
	0.75	516		256		176		765		241		333			192		483		1.74		0.26	
	1	531	513 [63] 472 [61]	268	305 [63] 270 [61]	148	141 [63] 145 [61]	786	806 [63] 726 [61]	264	282 [63] 243 [61]	330	333 [63] 310 [61]		204	193 [63] 191 [61]	508	485 [63] 669 [61]	1.61	1.73 [63] 1.62 [61]	0.24	0.26 [63] 0.20 [61]
WC-type	0	600	627 [58] 579 [59]	179	183 [58] 147 [59]	221	198 [58] 177 [59]	722	788 [58] 725 [59]	112	122 [58] 116 [59]	349	353 [58] 377 [59]		165	181 [58]	428	463 [58] 640 [59]	2.11	1.95 [58]	0.30	0.28 [58] 0.24 [59]
	0.25	600		175		201		732		129		341			178		455		1.91		0.28	
	0.5	606		181		179		752		143		337			189		478		1.78		0.26	
	0.75	618		188		172		760		182		339			211		524		1.61		0.24	
	1	635	611 [60] 616 [63] 556 [61]	203	341 [60] 212 [63] 205 [61]	147	184 [60] 142 [63] 152 [61]	804	884 [60] 818 [63] 737 [61]	232	221 [60] 256 [63] 222 [61]	340	378 [60] 337 [63] 318 [61]	351 [64]	239	220 [60] 243 [63] 213 [61]	580	554 [60] 588 [63] 676 [61]	1.42	1.72 [60] 1.39 [63] 1.49 [61]	0.22	0.26 [60] 0.21 [63] 0.20 [61]
TaN-type	0	341		324		219		494		50		300			34		98		8.85		0.45	
	0.5	419		267		189		563		114		299			106		286		2.81		0.34	
	0.75	466		240		180		598		151		303			142		368		2.14		0.30	
	1	525	538 [63]	210	238 [63]	163	165 [63]	655	665 [63]	186	191 [63]	308	319 [63]		182	182 [63]	456	4581 [63]	1.69	1.75 [63]	0.25	0.26 [63]

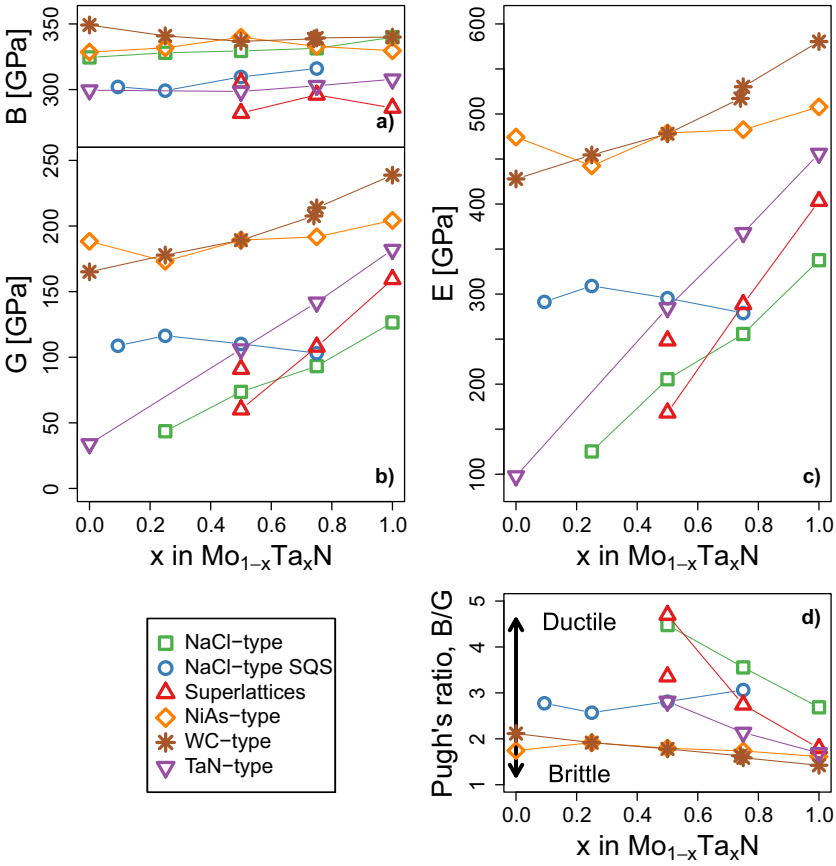

Fig. 8. (a) Bulk modulus, (b) shear modulus, and (c) Young's modulus of various $Mo_{1-x}Ta_xN$ solid solutions calculated as Hill's averages of Reuss's and Voigt's polycrystalline isotropic aggregates. (d) Pugh's ratio for estimating relative trends in brittleness/ductility.

are actually mechanically unstable, therefore, we do not show any data points) they provide the highest ductility of all polymorphs considered here. All three hexagonal modifications yield much lower B/G ratios, and thus are the most brittle structures considered here. Finally, we calculated Poisson's ratio, ν,

$$\nu = \frac{3B - 2G}{6B + 2G}, \tag{14}$$

and obtained comparable trends in ductile/brittle behavior (cf. Table II) by applying Frantsevich's criterion [70], which says that the material is brittle for $\nu < 1/3$.

3.5. Electronic density of states

Because the total density of electronic states, DOS, is non-zero at the Fermi level, E_F, all of our systems are metallic (Fig. 9), including the newly identified tetragonal ζ-phases. The energy region from −9 to about −4 eV can be characterized by strong hybridization of the Mo(Ta)-*d* electrons with the N-*p* electrons resulting in a dominant covalent bonding character [71–73]. The region from −4 eV to the Fermi level corresponds to the remaining metal *d* electrons. This behavior is well demonstrated by the fact that for every polymorph, the density of states of various compositions are alike; only E_F shifts due to accommodation of the extra electron (per formula unit) in MoN in comparison to TaN. This band filling leads, however, to pronounced changes around the Fermi level. All structures of TaN (but the cubic one) exhibit a local DOS minimum at E_F in the case of TaN. On the contrary, MoN even shows local DOS maximum (peak) for the cubic and hexagonal TaN-type structures. These trends are perfectly in line with the previously discussed mechanical (in)stability. Typically, a distinct peak at the Fermi level is an indicator for structural instability, while a local minimum at E_F suggests that the corresponding system is mechanically stable [74–77]. The disordered alloys show a noticeable increase of DOS around −1.5 eV together with a distinct minimum close to E_F (Fig. 9b). This is in strong contrast to the DOS of the ordered solid solutions (Fig. 9a). Therefore, also in terms of their electronic structure, the disordered cubic systems are found dissimilar to the ordered ones.

4. Conclusions

We have performed extensive DFT calculations on thermodynamic, structural, elastic, and electronic properties of $Mo_{1-x}Ta_xN$ alloys in their cubic (NaCl-type) and hexagonal (NiAs-, TaN- and WC-type) modifications. The role of atomic-scale architecture was analysed employing another concept of materials design—$(MoN)_{1-x}/(TaN)_x$ superlattices—with different layer thicknesses and MoN-to-TaN molar ratios.

Our calculations show that hexagonal alloys are the most stable ones over the whole compositional range, with a preference for the NiAs-, WC- and TaN-type structure for composition *x* in the range of 0–0.3, 0.3–0.9, and 0.9–1, respectively. Due to the comparable formation energies of WC- and TaN-type $Mo_{1-x}Ta_xN$ for *x* between 0.9 and 1, neither of the phases is strongly favoured and hence, specific parameters of deposition process (leading to, e.g., presence of point defects) may play a decisive role.

Within the metastable cubic systems, the disordered solid solutions and the superlattices are energetically strongly favoured over the ordered cubic $Mo_{1-x}Ta_xN$. Structural analysis (in terms of bond

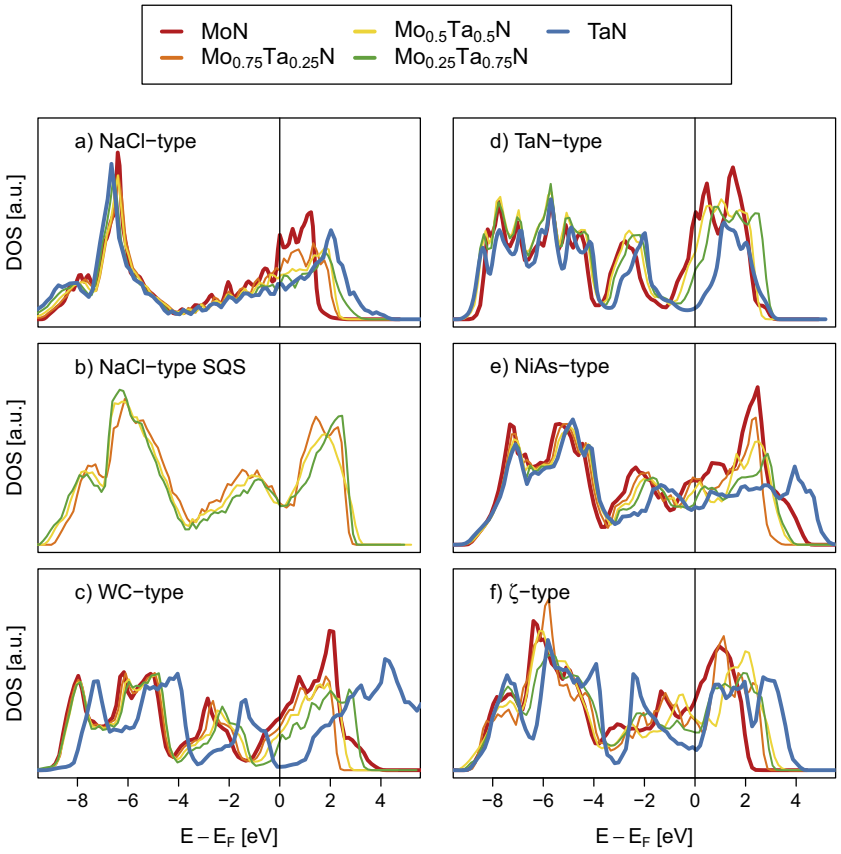

Fig. 9. Total density of electronic states, DOS [a.u.], for (a) ordered and (b) disordered NaCl-type, (c) WC-type, (d) TaN-type, (e) NiAs-type, and (f) ζ-type polymorphs of $Mo_{1-x}Ta_xN$ solid solutions.

lengths and angles) reveals that the disordered cubic systems exhibit local similarities with the hexagonal NiAs-type structure. As soon as Ta is introduced into cubic MoN in a disordered manner, the energy of formation significantly decreases due to these local hexagonal-like environments. Any further addition of Ta only leads to an almost linear change of E_f.

Also the $(MoN)_{1-x}/(TaN)_x$ superlattices immediately deviate from their cubic symmetry, and the MoN as well as TaN layers relax towards tetragonal ζ-phase (P4/nmm, #129). Formation energy of the newly uncovered ζ-MoN and ζ-TaN lie between that of the cubic and hexagonal binary polymorphs. Importantly, while the cubic TaN is vibrationally unstable, the ζ-TaN is stable, i.e., its phonon dispersion does not contain any imaginary phonon frequencies. The ζ-MoN still shows some soft phonons, however, the integrated phonon DOS corresponding to the imaginary frequencies yields fewer states than in the case of the cubic MoN. This suggests that ζ-MoN is an intermediate state towards a stable structure, which is stabilized by the superlattice.

To formulate design rules for MoTaN-based coatings, we established relations between elastic properties, Ta content, and architecture. The disordered cubic and all the hexagonal alloys are mechanically stable regardless Ta content. On the contrary, the ordered cubic systems and the superlattices fulfill conditions for mechanical stability only above a critical Ta content of ~25% and ~50%, respectively. Additional parameter controlling properties of $(MoN)_{1-x}/(TaN)_x$ superlattices is their bi-layer period which has to be set to ~2–3 nm in order to ensure mechanical stability. The polycrystalline elastic moduli suggest that the hexagonal NiAs- and WC-phases of $Mo_{1-x}Ta_xN$ are significantly harder than the other modifications. On the other hand, the superlattices and the cubic alloys are particularly interesting owning to their high ductility (according to Pugh's and Poisson's ratio). We hope that our systematic and detailed theoretical investigations on the quasi-binary MoN–TaN system will guide future experimental search for functional thin films with outstanding properties.

5. Data availability

The raw/processed data required to reproduce these findings cannot be shared at this time as the data also forms part of an ongoing study.

Acknowledgments

This research was supported by the START Program (Y371) of the Austrian Science Fund (FWF) [N.K., D.H., P.H.M.], by the Academy of Sciences of the Czech Republic through the Fellowship of J. E. Purkyně [M.F.], the Institutional Project No. RVO:68081723, by the Ministry of Education, Youth and Sports of the Czech Republic under the Project CEITEC 2020 (Project No. LQ1601) [M.F., M.Š.], and by the Czech Science Foundation (Project No. GA 16-24711S) [M.F., M.Š.]. Computational resources were provided by the Ministry of Education, Youth and Sports of the Czech Republic under the Projects CESNET (Project No. LM2015042), CERIT-Scientific Cloud (Project No. LM2015085), and IT4Innovations National Supercomputer Center (Project No. LM2015070) within the program Projects of Large Research, Development and Innovations Infrastructures [N.K., M.F., M.Š.]. Some calculations were carried out with the help of the Vienna Scientific Cluster (VSC) [D.H., N.K.].

References

[1] D. Holec, R. Rachbauer, L. Chen, L. Wang, D. Luef, P.H. Mayrhofer, Phase stability and alloy-related trends in Ti-Al-N, Zr-Al-N and Hf-Al-N systems from first principles, Surf. Coat. Technol. 206 (2011) 1698–1704.

[2] Y.X. Xu, H. Riedl, D. Holec, L. Chen, Y. Du, P.H. Mayrhofer, Thermal stability and oxidation resistance of sputtered TiAlCrN hard coatings, Surf. Coat. Technol. 324 (2017) 48–56.

[3] Y. Zou, X. Wang, T. Chen, X. Li, X. Qi, D. Welch, P. Zhu, B. Liu, T. Cui, B. Li, Hexagonal-structured ε-NbN: ultra-incompressibility, high shear rigidity, and a possible hard superconducting material, Sci. Rep. 5 (2015)srep10811.

[4] I. Jauberteau, A. Bessaudou, R. Mayet, J. Cornette, J.L. Jauberteau, P. Carles, T. Merle-Méjean, Molybdenum Nitride Films: Crystal Structures, Synthesis, Mechanical, Electrical and Some Other Properties, 2015.

[5] M. Zhang, K. Cheng, H. Yan, Q. Wei, B. Zheng, Electronic bonding analyses and mechanical strengths of incompressible tetragonal transition metal dinitrides TMN2 (TM= Ti, Zr, and Hf), Sci. Rep. 6 (2016)

[6] J. Musil, Hard nanocomposite coatings: thermal stability, oxidation resistance and toughness, Surf. Coat. Technol. 207 (2012) 50–65.

[7] N.P. Breznay, M. Tendulkar, L. Zhang, S.-C. Lee, A. Kapitulnik, Superconductor to weak-insulator transitions in disordered tantalum nitride films, 2017.arXiv preprint arXiv:1705.01732.

[8] M.R. Beebe, D.B. Beringer, M.C. Burton, K. Yang, R.A. Lukaszew, Stoichiometry and thickness dependence of superconducting properties of niobium nitride thin films, J. Vac. Sci. Technol. A 34 (2016) 021510.

[9] J. Simmendinger, U.S. Pracht, L. Daschke, T. Proslier, J.A. Klug, M. Dressel, M. Scheffler, Superconducting energy scales and anomalous dissipative conductivity in thin films of molybdenum nitride, Phys. Rev. B 94 (2016) 064506.

[10] L. Zhou, F.F. Klimashin, D. Holec, P.H. Mayrhofer, Structural and mechanical properties of nitrogen-deficient cubic Cr-Mo-N and Cr-W-N systems, Scr. Mater. 123 (2016) 34–37.

[11] F.F. Klimashin, H. Riedl, D. Primetzhofer, J. Paulitsch, P.H. Mayrhofer, Composition driven phase evolution and mechanical properties of Mo-Cr-N hard coatings, J. Appl. Phys. 118 (2015) 025305.

[12] P. Djemia, M. Benhamida, K. Bouamama, L. Belliard, D. Faurie, G. Abadias, Structural and elastic properties of ternary metal nitrides $Ti_xTa_{1-x}N$ alloys: first-principles calculations versus experiments, Surf. Coat. Technol. 215 (2013) 199–208.

[13] D. Holec, M. Friák, J. Neugebauer, P.H. Mayrhofer, Trends in the elastic response of binary early transition metal nitrides, Phys. Rev. B 85 (2012) 064101.

[14] F. Tasnadi, A.V. Lugovskoy, M. Odén, I.A. Abrikosov, Non-equilibrium vacancy formation energies in metastable alloys-a case study of $Ti_{0.5}Al_{0.5}N$, Mater. Des. 114 (2017) 484–493.

[15] M. Friák, D. Tytko, D. Holec, P. Choi, P. Eisenlohr, D. Raabe, J. Neugebauer, Synergy of atom-probe structural data and quantum-mechanical calculations in a theory-guided design of extreme-stiffness superlattices containing metastable phases, New J. Phys. 17 (2015) 093004.

[16] F. Pacher, P.H. Mayrhofer, D. Holec, Vacancy-driven extended stability of cubic metastable Ta-Al-N and Nb-Al-N phases, Surf. Coat. Technol. 326 (2017) 37–44.

[17] D. Music, R.W. Geyer, J.M. Schneider, Recent progress and new directions in density functional theory based design of hard coatings, Surf. Coat. Technol. 286 (2016) 178–190.

[18] O. Boudrifa, A. Bouhemadou, N. Guechi, S. Bin-Omran, Y. Al-Douri, R. Khenata, First-principles prediction of the structural, elastic, thermodynamic, electronic and optical properties of $Li_4Sr_3Ge_2N_6$ quaternary nitride, J. Alloys Compd. 618 (2015) 84–94.

[19] A. Bedjaoui, A. Bouhemadou, S. Aloumi, R. Khenata, S. Bin-Omran, Y. Al-Douri, F.S. Saoud, S. Bensalem, Structural, elastic, electronic and optical properties of the novel quaternary diamond-like semiconductors Cu_2MgSiS_4 and Cu_2MgGeS_4, Solid State Sci. 70 (2017) 21–35.

[20] Q. Li, L. Sha, C. Zhu, Y. Yao, New multifunctional tungsten nitride with energetic N6 and extreme hardness predicted from first principles, Europhys. Lett. 118 (2017) 46001.

[21] S. Veprek, M.G.J. Veprek-Heijman, Superhard and ultrahard nanostructured materials and coatings, Microstructure-Property Correlations for Hard, Superhard, and Ultrahard Materials, Springer. 2016, pp. 167–210.

[22] F.F. Klimashin, N. Koutná, H. Euchner, D. Holec, P.H. Mayrhofer, The impact of nitrogen content and vacancies on structure and mechanical properties of Mo-N thin films, J. Appl. Phys. 120 (2016) 185301.

[23] J. Lu, N. Arshi, Effects of Substrate bias on the hardness and resistivity of reactively sputtered TaN and TiN thin films, JOM 68 (2016) 1634–1639.

[24] S. Xu, P. Munroe, J. Xu, Z.-H. Xie, The microstructure and mechanical properties of tantalum nitride coatings deposited by a plasma assisted bias sputtering deposition process, Surf. Coat. Technol. 307 (2016) 470–475.

[25] D.M. Teter, Computational alchemy: the search for new superhard materials, MRS Bull. 23 (1998) 22–27.

[26] X. Chen, H. Niu, D. Li, Y. Li, Modeling hardness of polycrystalline materials and bulk metallic glasses, Intermetallics 19 (2011) 1275–1281.

[27] D. Li, F. Tian, D. Duan, K. Bao, B. Chu, X. Sha, B. Liu, T. Cui, Mechanical and metallic properties of tantalum nitrides from first-principles calculations, RSC Adv. 4 (2014) 10133–10139.

[28] K. Balasubramanian, L. Huang, D. Gall, Phase stability and mechanical properties of $Mo_{1-x}N_x$ with $0 \le x \le 1$, J. Appl. Phys. 122 (2017) 195101.

[29] J. Haines, J.M. Leger, G. Bocquillon, Synthesis and design of superhard materials, Annu. Rev. Mater. Res. 31 (2001) 1–23.

[30] P.H. Mayrhofer, R. Rachbauer, D. Holec, F. Rovere, J.M. Schneider, Protective transition metal nitride coatings, 2014.

[31] S. Wang, D. Antonio, X. Yu, J. Zhang, A.L. Cornelius, D. He, Y. Zhao, The hardest superconducting metal nitride, Sci. Rep. 5 (2015)

[32] B.D. Ozsdolay, K. Balasubramanian, D. Gall, Cation and anion vacancies in cubic molybdenum nitride, J. Alloys Compd. 705 (2017) 631–637.

[33] T. Mashimo, S. Tashiro, M. Nishida, K. Miyahara, E. Eto, B1-type and WC-type phase bulk bodies of tantalum nitride prepared by shock and static compressions, Phys. B Condens. Matter 239 (1997) 13–15.

[34] B. Bouaouina, A. Besnard, S.E. Abaidia, A. Airoudj, F. Bensouici, Correlation between mechanical and microstructural properties of molybdenum nitride thin films deposited on silicon by reactive RF magnetron discharge, Surf. Coat. Technol. 333 (2018) 32–38.

[35] N. Haberkorn, S. Bengio, S. Suárez, P. Pérez, M. Sirena, J. Guimpel, Effect of the nitrogen-argon gas mixtures on the superconductivity properties of reactively sputtered molybdenum nitride thin films, Mater. Lett. 215 (2018) 15–18.

[36] K. Bouamama, P. Djemia, M. Benhamida, First-principles calculation of the structural and elastic properties of ternary metal nitrides $Ta_xMo_{1-x}N$ and $Ta_xW_{1-x}N$, Journal of Physics: Conference Series, vol. 640, IOP Publishing. 2015, pp. 012022.

[37] X. Junhua, X. Yaping, C. Jun, Y. Lihua, Microstructures, mechanical and friction properties of TaMoN composite films, Rare Metal Mater. Eng. 43 (2014) 1412–1416.

[38] S.-H. Wei, L.G. Ferreira, J.E. Bernard, A. Zunger, Electronic properties of random alloys: special quasirandom structures, Phys. Rev. B 42 (1990) 9622–9649.

[39] G. Kresse, J. Furthmüller, Efficient iterative schemes for *ab initio* total-energy calculations using a plane-wave basis set, Phys. Rev. B 54 (1996) 11169–11186.

[40] G. Kresse, D. Joubert, From ultrasoft pseudopotentials to the projector augmented-wave method, Phys. Rev. B 59 (1999) 1758–1775.

[41] W. Kohn, L.J. Sham, Self-consistent equations including exchange and correlation effects, Phys. Rev. 140 (1965) A1133–A1138.

[42] J.P. Perdew, K. Burke, M. Ernzerhof, Generalized gradient approximation made simple, Phys. Rev. Lett. 77 (1996) 3865–3868.

[43] K. Momma, F. Izumi, An integrated three-dimensional visualization system VESTA using wxWidgets, Commission on Crystallogr. Comput., IUCr Newsl. 7 (2006) 106.

[44] K. Momma, F. Izumi, VESTA: a three-dimensional visualization system for electronic and structural analysis, J. Appl. Crystallogr. 41 (2008) 653.

[45] K. Momma, F. Izumi, VESTA 3 for three-dimensional visualization of crystal, volumetric and morphology data, J. Appl. Crystallogr. 44 (2011) 1272.

[46] F. Birch, Finite elastic strain of cubic crystals, Phys. Rev. 71 (1947) 809–824.

[47] Y. Le Page, P. Saxe, Symmetry-general least-squares extraction of elastic data for strained materials from ab initio calculations of stress, Phys. Rev. B 65 (2002) 104104.

[48] Y. Le Page, P. Saxe, Symmetry-general least-squares extraction of elastic coefficients from ab initio total energy calculations, Phys. Rev. B 63 (2001) 174103.

[49] M. Moakher, A.N. Norris, The closest elastic tensor of arbitrary symmetry to an elasticity tensor of lower symmetry, J. Elast. 85 (2006) 215–263.

[50] J.T. Browaeys, S. Chevrot, Decomposition of the elastic tensor and geophysical applications, Geophys. J. Int. 159 (2004) 667–678.

[51] F. Mouhat, F.-X. Coudert, Necessary and sufficient elastic stability conditions in various crystal systems, Phys. Rev. B 90 (2014) 224104.

[52] A. Togo, F. Oba, I. Tanaka, First-principles calculations of the ferroelastic transition between rutile-type and $CaCl_2$-type SiO_2 at high pressures, Phys. Rev. B 78 (2008) 134106.

[53] A.R. Denton, N.W. Ashcroft, Vegard's law, Phys. Rev. A 43 (1991) 3161.

[54] L. Vegard, Die konstitution der mischkristalle und die raumfüllung der atome, Z. Phys. 5 (1921) 17–26. (In German.).

[55] N. Koutná, D. Holec, O. Svoboda, F.F. Klimashin, P.H. Mayrhofer, Point defects stabilise cubic Mo-N and Ta-N, J. Phys. D. Appl. Phys. 49 (2016) 375303.

[56] D. Holec, D. Legut, L. Isaeva, P. Souvatzis, H. Clemens, S. Mayer, Interplay between effect of Mo and chemical disorder on the stability of β/β_0-TiAl phase, Intermetallics 61 (2015) 85–90.

[57] J. Nye, Physical Properties of Crystals, Clarendon Press, Oxford, 1957.

[58] E. Zhao, J. Wang, Z. Wu, Displacive phase transition, structural stability, and mechanical properties of the ultra-incompressible and hard MoN by first principles, Phys. Status Solidi B 247 (2010) 1207–1213.

[59] M.B. Kanoun, S. Goumri-Said, M. Jaouen, Structure and mechanical stability of molybdenum nitrides: a first-principles study, Phys. Rev. B 76 (2007) 134109.

[60] J. Chang, G.-P. Zhao, X.-L. Zhou, K. Liu, L.-Y. Lu, Structure and mechanical properties of tantalum mononitride under high pressure: a first principles study, J. Appl. Phys. 112 (2012)

[61] J. Li, X. Wang, K. Liu, D. Li, L. Chen, Crystal structures, mechanical and electronic properties of tantalum monocarbide and mononitride, J. Superhard Mater. 33 (2011) 173–178.

[62] E. Soignard, O. Shebanova, P.F. McMillan, Compressibility measurements and phonon spectra of hexagonal transition-metal nitrides at high pressure: ε-TaN, δ-MoN, and Cr 2 N, Phys. Rev. B 75 (2007) 014104.

[63] E. Zhao, B. Hong, J. Meng, Z. Wu, First principles investigation on the ultra-incompressible and hard TaN, J. Comput. Chem. 30 (2009) 2358–2363.

[64] H. Yusa, F. Kawamura, T. Taniguchi, N. Hirao, Y. Ohishi, T. Kikegawa, High–pressure synthesis and compressive behavior of tantalum nitrides, J. Appl. Phys. 115 (2014) 103520.

[65] R. Hill, The elastic behaviour of a crystalline aggregate, Proc. Phys. Soc. Sect. A 65 (1952) 349.
[66] A. Reuss, Berechnung der fließgrenze von mischkristallen auf grund der plastizitätsbedingung für einkristalle., ZAMM J. Appl. Math. Mech. (Z. Angew. Math. Mech.) 9 (1929) 49–58. (In German.).
[67] W. Voigt, in: B.G. Teubner, J.W. Edwards (Eds.), Lehrbuch der Kristallphysik (mit Ausschluss der Kristalloptik), 1928, Leipzig BerlinAnn, Arbor, Mich (In German.).
[68] F. Tasnádi, M. Odén, I.A. Abrikosov, Ab initio elastic tensor of cubic $Ti_{0.5}Al_{0.5}N$ alloys: dependence of elastic constants on size and shape of the supercell model and their convergence, Phys. Rev. B 85 (2012) 144112.
[69] S.F. Pugh, Relations between the elastic moduli and the plastic properties of polycrystalline pure metals, Lond. Edinb. Dublin Philos. Mag. J. Sci. 45 (1954) 823–843.
[70] I.N. Frantsevich, F.F. Voronov, S.A. Bokuta, I.N. Frantsevich, Elastic constants and elastic moduli of metals and insulators handbook, Naukova Dumka, Kiev, 1983, 60.
[71] B. Alling, A.V. Ruban, A. Karimi, O.E. Peil, S.I. Simak, L. Hultman, I.A. Abrikosov, Mixing and decomposition thermodynamics of c-$Ti_{1-x}Al_xN$ from first-principles calculations, Phys. Rev. B 75 (2007) 045123.
[72] R. Rachbauer, D. Holec, M. Lattemann, L. Hultman, P.H. Mayrhofer, Electronic origin of structure and mechanical properties in Y and Nb alloyed Ti-Al-N thin films, Int. J. Mater. Res. 102 (2011) 735–742.
[73] F. Rovere, D. Music, S. Ershov, M. to Baben, H.-G. Fuss, P.H. Mayrhofer, J.M. Schneider, Experimental and computational study on the phase stability of Al-containing cubic transition metal nitrides, J. Phys. D. Appl. Phys. 43 (2010) 035302.
[74] M. Friák, M. Šob, V. Vitek, Ab initio study of the ideal tensile strength and mechanical stability of transition-metal disilicides, Phys. Rev. B 68 (2003) 184101.
[75] D. Legut, M. Friák, M. Šob, Phase stability, elasticity, and theoretical strength of polonium from first principles, Phys. Rev. B 81 (2010) 214118.
[76] M. Zelený, M. Friák, M. Šob, Ab initio study of energetics and magnetism of Fe, Co, and Ni along the trigonal deformation path, Phys. Rev. B 83 (2011) 184424.
[77] L.-F. Zhu, M. Friák, A. Dick, B. Grabowski, T. Hickel, F. Liot, D. Holec, A. Schlieter, U. Kuehn, J. Eckert, Z. Ebrahimi, H. Emmerich, J. Neugebauer, First-principles study of the thermodynamic and elastic properties of eutectic Fe-Ti alloys, Acta Mater. 60 (2012) 1594–1602.